

1 **Two New Polymorphic Cocrystals of Zafirlukast: Preparation, Crystal Structure, and Stability**  
2 **Relations**

3  
4  
5  
6 Antonio Llinas,<sup>\*,‡</sup> Rafael Barbas,<sup>†</sup> Mercè Font-Bardia,<sup>†</sup> Michael J. Quayle,<sup>§</sup> Sitaram Velaga,<sup>⊥</sup> and  
7 Rafel Prohens<sup>\*,†,||</sup>  
8  
9  
10  
11  
12  
13  
14  
15  
16  
17  
18  
19  
20

21 <sup>‡</sup>R&D AstraZeneca, Respiratory, Inflammation and Autoimmune iMed, Pepparedsleden 1, SE-431 83,  
22 Mölndal, Sweden

23 <sup>†</sup>Unitat de Polimorfisme i Calorimetria and Unitat de Difracció de Raigs X, Centres Científics i  
24 Tecnològics, Universitat de Barcelona,  
25 Baldiri Reixac 10, 08028 Barcelona, Spain

26 <sup>§</sup>R&D AstraZeneca, Global Medicines Development, Pharmaceutical Development, Pepparedsleden 1,  
27 SE-431 83, Mölndal, Sweden

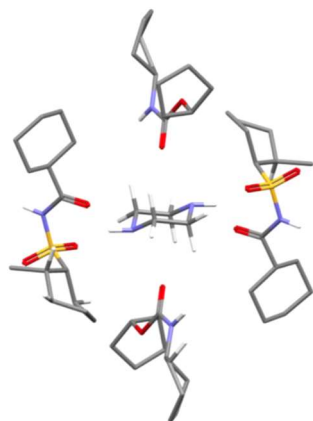
28 <sup>⊥</sup>Department of Health Sciences, Luleå University of Technology, SE-971 87 Luleå, Sweden

29 <sup>||</sup>Center for Intelligent Research in Crystal Engineering S.L, Palma de Mallorca 07121, Spain  
30  
31  
32  
33  
34  
35  
36  
37  
38  
39  
40  
41  
42  
43  
44

45 **ABSTRACT**

46

47 Two new cocrystals of zafirlukast with piperazine, existing in five different solid forms, have been  
48 discovered during a cocrystal screening. The crystal structure of one of these forms has been determined  
49 by single crystal X-ray diffraction, and the stability landscape of the crystalline forms of the new  
50 cocrystal has been studied. In the present article, we extend the knowledge about the solid state of this  
51 important pharmaceutical drug for the treatment of asthma by reporting the crystal structures of two new  
52 solvates (acetonitrile and butanol) and the elusive anhydrous Form X, which have been solved by single  
53 crystal X-ray diffraction.



54

55

56

57

58

59

60

## 61 1. INTRODUCTION

62

63 The design and synthesis of cocrystals of active pharmaceutical ingredients (APIs) have attracted much  
64 interest recently due to their potential ability to modify important properties of pharmaceutical materials  
65 such as solubility or stability, which can be improved with respect to the native active compound.<sup>1</sup> Also,  
66 the investigation of polymorphism of APIs is a key issue because of its great impact not only on the  
67 chemical properties but also on the intellectual property related to the commercial exploitation of a  
68 drug.<sup>2</sup> Cocrystals can exhibit polymorphism or pseudo-polymorphism (presence of solvent molecules in  
69 the crystal structure) in the same way as single-component crystalline solids, and thus they must be  
70 completely characterized prior to a defensive strategy, which eventually will take the form of a patent.<sup>3</sup>  
71 Moreover, cocrystallization can provide the way to increase the number of solid forms for an API  
72 through stoichiometric variations between the different components that form the cocrystal.<sup>4</sup>

73 In this sense, the number of cocrystals with different API/coformer stoichiometries and their mutual  
74 interconversion, the presence of polymorphism, the stability of solvates, and their conversion to pure  
75 forms upon solvent removal must be known in order to design the experimental conditions for the  
76 selective preparation of the desired crystal form.

77 Zafirlukast, (4-(5-cyclopentyloxycarbonylamino-1-methylindol-3-ylmethyl)-3-methoxy-o-toyl  
78 sulphonylbenzamide, ZF hereafter, Figure 1), is a cysteinyl leukotriene which is used to help to control  
79 the symptoms of asthma.<sup>5</sup> ZF has been described previously to exist in five crystal modifications: the  
80 anhydrous form,<sup>6</sup> an acetonitrile solvate,<sup>7</sup> a methanol solvate,<sup>8</sup> an ethanol solvate,<sup>8</sup> and a  
81 monohydrate,<sup>6</sup> with only the crystal structure of the last three forms already reported,<sup>8</sup> and the crystal  
82 structure of the anhydrous form remains, so far, elusive.

83 The anhydrous form of ZF shows relatively low bioavailability, and hence the amorphous form is  
84 selected for further development in the industry. The amorphous form of ZF has relatively good physical  
85 stability and bioavailability and is prepared by dehydration of the monohydrate form in a vacuum oven  
86 at 393 K for 24 h.<sup>9</sup> However, amorphous ZF can convert to the monohydrate (which has low  
87 bioavailability) in the presence of water. Thus, new crystalline forms with potential improved  
88 bioavailability over the anhydrous form are attractive for this API.

89 In this article, we present two polymorphic cocrystals of ZF with piperazine together with the  
90 description of the relative stability of its forms and the crystal structure of the 2:1 (ZF:piperazine)  
91 cocrystal. The study includes the first reported crystal structure of the anhydrous form of ZF and two  
92 novel solvate forms. A comparative analysis of the intermolecular interactions present in all four new  
93 crystal structures of this oral drug is also presented.

94

95 **2. MATERIALS AND METHODS**

96

97 **2.1. Synthesis of the Different Crystal Forms.** 2.1.1. Anhydrous Form X. It was obtained by slow  
98 crystallization at room temperature from a non saturated solution of ZF in IPA, pentane, heptane,  
99 cyclohexane, toluene, xylene, AcOEt, Et<sub>2</sub>O, ethylene glycol dimethyl, diisopropyl ether, or  
100 dichloromethane (m.p. 190 °C).

101 2.1.2. Butanol Solvate. It was obtained by slow crystallization from a solution of ZF (20 mg) in BuOH  
102 (3.0 mL) at 80 °C. The solution was cooled down at room temperature in 30 min and crystals appeared  
103 after 2 days.

104 2.1.3. Acetonitrile Solvate. It was obtained by slow crystallization from a solution of ZF (15 mg) in  
105 ACN (1.3 mL) at 50 °C. The solution was cooled down at room temperature in 30 min and crystals  
106 appeared after 2 days.

107 2.1.4. Piperazine Cocrystal (2:1) Form A. It was obtained by slow crystallization from a solution of  
108 ZF:piperazine (1:1) in ethanol. ZF (20 mg) and piperazine (3 mg), molar ratio 1:1, were dissolved in  
109 ethanol (0.3 mL) at 60 °C. The solution was cooled down at room temperature in 30 min and crystals  
110 appeared after 4 days (m.p. 218 °C).

111 2.1.5. Piperazine Cocrystal (2:1) Form B. It was obtained by slurry in water at room temperature. ZF (50  
112 mg) and piperazine (11 mg), molar ratio 1:1.5, were slurred in water (0.4 mL) at room temperature  
113 during 24 h. The solid was filtered and dried under a vacuum 48 h, (m.p. 212 °C).

114 2.1.6. Piperazine Cocrystal (1:1) Form C. It was obtained by slurry in ethanol at room temperature. ZF  
115 (75 mg) and piperazine (20 mg), molar ratio 1:2, were slurred in ethanol (0.05 mL) at room temperature  
116 during 24 h. The solid was filtered and dried under vacuum 48 h.

117 2.1.7. Piperazine Cocrystal (1:1) Form D. It was obtained by slurry in methanol, IPA, acetonitrile,  
118 acetone, MiBK or AcOEt at room temperature. For instance, ZF (50 mg) and piperazine (11 mg), molar  
119 ratio 1:1.5, were slurred in ACN (1.0 mL) at room temperature during 24 h. The solid was filtered and  
120 dried under vacuum 48 h, (mp 181 °C).

121 2.1.8. Piperazine Cocrystal (1:1) Toluene Solvate Form E. It was obtained by slurry in toluene at room  
122 temperature. ZF (50 mg) and piperazine (11 mg), molar ratio 1:1.5, were slurred in toluene (1.0 mL) at  
123 room temperature during 24 h. The solid was filtered and dried under vacuum 48 h, (mp 106 °C).

124 **2.2. Methods.** 2.2.1. Powder X-ray Diffraction (PXRD). Powder Xray diffraction patterns were obtained  
125 on a PANalytical X'Pert PRO MPD diffractometer in transmission configuration using Cu K $\alpha$ 1 + 2  
126 radiation ( $\lambda = 1.5418 \text{ \AA}$ ) with a focalizing elliptic mirror, a PIXcel detector working at a maximum  
127 detector's active length of 3.347°. Capillary geometry has been used with samples placed in glass  
128 capillaries (Lindemman) of 0.5 mm of diameter measuring from 2 to 60° in 2 $\theta$ , with a step size of  
129 0.026° and a total measuring time of 30 min. Flat geometry has been used for routine samples  
130 sandwiched between low absorbing films (polyester of 3.6  $\mu\text{m}$  of thickness) measuring 2 $\theta$ / $\theta$ scans from 2  
131 to 40° in 2 $\theta$  with a step size of 0.026° and a measuring time of 76 s per step. When cell indexation was  
132 required, the powder X-ray diffraction pattern was obtained using capillary geometry and soller slit of  
133 0.01 radians. The sample was placed in a capillary of 0.7 mm, and consecutive 2 $\theta$  scans from 2 to 70°  
134 were measured and added.

135 2.2.2. Single Crystal X-ray Diffraction. Two different instruments have been used. (a) MAR345  
136 diffractometer with an image plate detector was used. Intensities were collected with graphite  
137 monochromatized MoK $\alpha$  radiation ( $\lambda = 0.71073 \text{ \AA}$ ) using a  $\phi$ -scan technique. The structures were

138 solved by direct methods, using the SHELXS computer program<sup>10</sup> and refined by full-matrix least-  
139 squares method with the SHELX97 computer program.

140 (b) A D8 Venture system equipped with a multilayer monochromator and a Mo microfocus ( $\lambda = 0.71073$   
141 Å) was used too. Frames were integrated with the Bruker SAINT software package using a SAINT  
142 algorithm. Data were corrected for absorption effects using the multiscan method (SADABS). The  
143 structure was solved and refined using the Bruker SHELXTL Software Package,<sup>11</sup> a computer program  
144 for automatic solution of crystal structure and refined by fullmatrix least-squares method with ShelXle  
145 Version 4.8.0, a Qt graphical user interface for SHELXL computer program.<sup>12</sup>

146 2.2.3. Differential Scanning Calorimetry (DSC). Differential scanning calorimetry was carried out by  
147 means of a Mettler-Toledo DSC-822e calorimeter. Experimental conditions: aluminum crucibles of 40  
148 µL volume, atmosphere of dry nitrogen with 50 mL/min flow rate, heating rate of 10 °C/min. The  
149 calorimeter was calibrated with indium of 99.99% purity.

150 2.2.4. Thermogravimetric Analysis (TGA). Thermogravimetric analyses were performed on a Mettler-  
151 Toledo TGA-851e thermobalance. Experimental conditions: alumina crucibles of 70 µL volume,  
152 atmosphere of dry nitrogen with 50 mL/min flow rate, heating rate of 10 °C/min.

153 2.2.5. Cocrystal Screening. Screening for cocrystal formation through liquid assisted grinding  
154 experiments (LAG) was conducted by grinding 20–30 mg of a 1:1 mixture of ZF and each conformer  
155 together with one drop of different solvents using a Retsch MM 2000 grinding mill. The samples were  
156 placed in 2 mL volume stainless steel jars, along with two stainless tungsten grinding balls of 3 mm  
157 diameter. Grinding was performed for 15–30 min, with a frequency of the mill of 30 Hz. Finally, the  
158 samples were collected immediately without prior drying for PXRD analysis. The formation of a  
159 cocrystal was determined by comparing PXRD patterns of starting materials and products from cocrystal  
160 screening LAG experiments.

161

162

### 163 3. RESULTS AND DISCUSSION

164

165 3.1. Solid Forms Screening of ZF. Bearing in mind that only an anhydrous form has been described for  
166 ZF, we conducted a polymorph screening starting from the amorphous material in order to obtain and  
167 characterize as many forms as possible. Using a broad set of thermodynamic and kinetic crystallization  
168 conditions from a variety of solvents, we obtained evidence of solvate formation with methylethylketone,  
169 acetone, methylisobutylketone, benzyl alcohol, ammonia, acetonitrile, and butanol. However, we could  
170 only isolate in pure form the last two solvates. A summary of all experimental conditions can be found  
171 in the Supporting Information section. All forms were characterized by means of X-ray powder  
172 diffraction, DSC, and TGA. The X-ray powder diffractograms of the new solvates (compared with the  
173 anhydrous Form X) are shown in Figure 2, while Figures 3 and 4 show the DSC and the TGA curves of  
174 the different solvates, respectively.

175 No new anhydrous polymorphs were detected. In all cases the DSC thermograms show a very similar  
176 pattern of desolvation on heating followed by the crystallization and subsequent melting of the  
177 anhydrous form. All desolvated samples were analyzed by PXRD, and the transformation into the  
178 anhydrous Form X was confirmed.

179 3.2. Cocrystal Screening. Since ZF contains strong Hbond donor and acceptor groups, a diverse set of  
180 cofomers such as amines, alcohols, and carboxylic acids, among others, were selected having  
181 acceptable toxicity profiles. Supporting Information contains the complete list of cofomers tested in this  
182 study. The analysis by PXRD of the samples generated during the LAG experiments revealed that 4 out  
183 of the 25 tested cofomers showed evidence of the existence of new solid phases different than any  
184 known form of ZF and the respective cofomer: 3-hydroxybenzoic acid, 3,4-dihydroxybenzoic acid, 4-  
185 hexylresorcinol, and piperazine. However, although great efforts were devoted to isolate the new solid  
186 forms, only piperazine produced pure new forms suitable for further characterization and analysis. The  
187 following section describes them in detail.

188 3.3. Crystal Structures Analysis. 3.3.1. Anhydrous Form X of Zafirlukast. Anhydrous Form X  
189 crystallizes with one molecule of ZF in the asymmetric unit forming ribbons linked through  
190 amide–amide hydrogen-bond interactions. The structure shows a pattern of hydrogen-bond interactions  
191 following the expected hierarchical order between the best donor<sup>13</sup> (sulphonylbenzamide NH) and the  
192 best acceptor (amide CO) together with the second best donor (amide NH) and the second best acceptor  
193 (sulphonylbenzamide CO) with an alternate amide/sulphonylamide supramolecular synthon (Figure 5).

194 Ribbons are connected through weak CH $\cdots\pi$  interactions between a methoxy group and an aromatic  
195 ring (Cmethoxy–H $\cdots\pi$  centroid distance of 3.20 Å), Figure 6a and between two aromatic rings  
196 (Carene–H $\cdots\pi$  centroid distance of 2.65 Å), Figure 6b.

197 3.3.2. Zafirlukast Acetonitrile Solvate. ZF acetonitrile solvate crystallizes with one molecule of ZF and  
198 one of acetonitrile in the asymmetric unit. Interestingly, no hydrogenbonding chains or ribbons are  
199 formed but discrete dimers of ZF molecules linked through a combination of amide–amide hydrogen-  
200 bond interactions between the best donor (sulphonylbenzamide NH) and the best acceptor (amide CO)  
201 groups together with weak CH $\cdots\pi$  interactions involving the methoxy groups. Two molecules of  
202 acetonitrile surround each ZF dimer forming strong hydrogen bonds with the second best donor groups  
203 of ZF (amide NH) conferring extra stability to the selfassembled dimers (Figure 7).

204 3.3.3. Zafirlukast Butanol Solvate. ZF butanol solvate also crystallizes with one molecule of ZF and one  
205 of butanol in the asymmetric unit. Infinite chains of ZF molecules are formed through strong hydrogen  
206 bonds but in a very different way with respect to the anhydrous Form X. Butanol molecules establish  
207 hydrogen bonds simultaneously with the best donor and the best acceptor of ZF leaving free the second  
208 best donor and the second best acceptor to form chains of self-assembled ZF molecules, Figures 8 and 9.

209 Layers are interconnected through weak CH $\cdots\pi$  interactions involving different protons of the  
210 methylindole group of ZF, (Carene–H $\cdots\pi$  centroid distance of 2.84 and 3.20 Å), Figure 10, an  
211 interaction not observed in the other forms of ZF.

212 3.3.4. Cocrystal Zafirlukast/Piperazine (2:1). In the crystal structure, different supramolecular synthons  
213 are observed with respect to the other structures of ZF. The main difference is that the oxygens of the  
214 benzenesulphonyl groups are involved in hydrogen bonds with the NH proton of the amide moiety. Very  
215 interestingly, this amide group has an infrequent cis conformation. It is well-known that acyclic  
216 secondary amides are usually found in the most stable trans amide conformation; however there is  
217 literature evidence that the equilibrium toward the less stable cis conformation can occur when strong  
218 noncovalent interactions are present.<sup>14</sup> For example, many proteins have amino acid residues in a cis  
219 conformation because C–H $\cdots\pi$  interactions are able to stabilize them.<sup>15</sup> Moreover, it has been observed  
220 that the replacement of the N-alkyl substituent of a secondary amide by a phenyl group tends to increase  
221 the stability of the cis conformer.<sup>16</sup>

222 Although piperazine is a molecule which plays important roles in several fields, such as enzyme  
223 inhibitors,<sup>17</sup> liquid crystalline compounds<sup>18</sup> or recreative drugs,<sup>19</sup> only 12 crystal structures of  
224 piperazine in neutral form have been described so far.<sup>20</sup>

225 In the cocrystal structure, the piperazine resides on a crystallographic inversion center and has the most  
226 stable chair conformation with NH protons in the equatorial positions. Each piperazine occupies the  
227 space formed by four ZF molecules with six H-bond donors pointing to the center of the cavity. Since  
228 the piperazine has two strong donor and two acceptor groups, its location into the cavity is held by a  
229 favorable balance between attractive and repulsive interactions with the six donor groups, Figure 12.

230 **3.4. Polymorphism of the Piperazine Cocrystal.** Usually the most stable polymorphic modification is  
231 used in a marketed formulation. Overlooking the most stable polymorph may cause failure of a  
232 marketed product, because a phase transformation during storage can occur. A lateappearing stable  
233 polymorph can have a negative impact on development timelines<sup>21</sup> as it has been shown by many  
234 reviews written on disappearing polymorphs.<sup>22</sup> However, metastable forms may survive years if a high  
235 activation energy barrier has to be overcome in moving from the metastable form to the stable one. In  
236 the present case, some information about the stability and interconversion of the different ZF/piperazine  
237 cocrystals has been obtained.

238 Five different forms of a multicomponent crystal formed by ZF and piperazine were discovered and  
239 isolated during the cocrystal screen: three forms with 1:1 stoichiometry (including a toluene solvate) and  
240 two forms with 2:1 stoichiometry. Figures 13 and 14 show the PXRD patterns of these five forms.

241 As it has been described previously, only one of the two 2:1 cocrystal structures has been solved by  
242 single crystal XRD (Form A). However, the cell of the second polymorph (Form B) has been indexed  
243 (Figures of Merit of M: 25; F: 75. Unit cell parameters were refined by Le Bail fit<sup>23</sup> using Fullprof  
244 program<sup>24</sup> with a final  $\chi^2$ : 4.75), being also triclinic with similar cell dimensions and a slightly bigger  
245 volume (Figure 15 and Table 1). The higher density of Form A suggests that Form B is metastable at  
246 room temperature with respect to Form A, which was confirmed through solvent mediated  
247 transformation experiments: a mixture of Form A and Form B transforms into pure Form A after 72 h  
248 slurring in ethanol.

249 But in order to complete the stability landscape, it is necessary to define whether the two forms are  
250 monotropically (one form is more stable than the other at any temperature) or enantiotropically (a  
251 transition temperature exists, where the stability order is reversed) related. DSC provides information  
252 about the melting temperature and the enthalpy of fusion of each form, which can be analyzed to define  
253 the relative stability between the two polymorphs. Thus, according to the so-called “heat-of-fusion  
254 rule”,<sup>25</sup> Forms A and B are monotropically related (Form A is thermodynamically more stable than

255 Form B at all temperatures up to the melting point) since Form A has the highest melting point and  
256 highest enthalpy of fusion (Table 2).

257 On the other hand, the three 1:1 cocrystal forms tend to transform into the apparently more stable 2:1  
258 cocrystal and reduce the content of piperazine. For instance, Form C transforms into Form B after 6  
259 months at room temperature, and Forms D and E transform into Form B after 48 h slurring in water.  
260 Interestingly, when Form C is heated up it shows a loss on weight around 120 °C, and the melting of the  
261 2:1 cocrystal is observed, Figure 16. PXRD analysis confirms Form B is obtained. The fact that the DSC  
262 curves of the two polymorphs of the 2:1 cocrystals do not show the loss of piperazine until they melt  
263 suggests that there are two different crystallographic positions of the piperazine molecules in the  
264 structures of the 1:1 cocrystals, one labile enough to be disturbed upon heating and another strong  
265 enough to resist until melting at very high temperature. Unfortunately, since the crystal structure of any  
266 of the 1:1 cocrystals remains elusive this hypothesis is rather speculative.

267



268 **4. CONCLUSION**

269

270 A spectroscopist from Chicago (Walter McCrone) said in 1965 that the number of polymorphs a  
271 compound has is proportional to the amount of money and time that has been spent investigating the  
272 molecule.<sup>26</sup> In the case of cocrystals this is also true, but pharmaceutical cocrystal development is by no  
273 means a straightforward process. To engineer the right cocrystal requires not only a deep knowledge of  
274 the intermolecular forces present in the cocrystal and crystal packing, but also finding the right set of  
275 conditions for which the sum of the chemical potentials of the components in solution is greater than in  
276 the solid phases, implying prediction of activity coefficients and knowledge of ternary solubility data.<sup>27</sup>  
277 High throughput screening is usually performed trying to maximize the potential to find new cocrystals,  
278 but given the number of variables involved it is difficult to cover the full landscape.

279 From the pharmaceutical point of view spending money and time in the discovery of new cocrystals will  
280 only make sense if the new cocrystal has some kind of advantage, of clinical relevance (i.e., improved  
281 human pharmacokinetics through changes in solubility and/or dissolution rates, a better toxicity profile  
282 (lower C<sub>max</sub>/C<sub>min</sub>), improved solid state properties such as stability, crystalline form/habit,  
283 processability or developability), over the parent API itself. At present, the predictability of the physical  
284 chemistry properties of a cocrystal is still far from ideal,<sup>28</sup> and the impact of these physicochemical  
285 properties changes on the pharmacokinetics is still not well understood because the amount of cocrystal  
286 PK data in the literature is insufficient to do a proper quantitative analysis.<sup>28</sup>

287 A first step in the ultimate goal of understanding the cocrystal behavior in vivo, and hence, being able to  
288 predict it, is the generation of new cocrystals (properly characterized) of medicines already on the  
289 market, so all the data generated can be openly shared within the scientific community. With this  
290 intention we have explored thoroughly the solid form landscape of ZF. The four new forms found  
291 (anhydrous, solvate, and cocrystal forms) show a rich diversity of intermolecular interactions. Thus, it is  
292 not surprising that the first reported cocrystal of this important API exists in at least five different forms  
293 with two stoichiometries, converting ZF in another example of the increasing list of compounds capable  
294 to form polymorphic cocrystals.<sup>29</sup> These new forms have been carefully characterized and will be the  
295 subject of a future investigation addressing the relationships between physical chemistry properties and  
296 the cocrystal pharmacokinetics. These results will be the subject of future contributions.

297

298

299 **AUTHOR INFORMATION**

300 **Corresponding Authors**

301 \*(A.L.) E-mail: [antonio.llinas@astrazeneca.com](mailto:antonio.llinas@astrazeneca.com).

302 \*(R.P.) E-mail: [rafel@ccit.ub.edu](mailto:rafel@ccit.ub.edu).

303

304 **Notes**

305 The authors declare no competing financial interest

306

307

308

309

310 **REFERENCES**

311

312 (1) Blagden, N.; de Matas, M.; Gavan, P. T.; York, P. *Adv. Drug Delivery Rev.* 2007, 59, 617–630.

313 (2) Hilfiker, R. *Polymorphism in the Pharmaceutical Industry*; Wiley-VCH: Weinheim, 2006.

314 (3) Shattock, T. R.; Vishweshwar, P.; Wang, Z.; Zaworotko, M. J. *Cryst. Growth Des.* 2005, 5,  
315 2046–2049.

316 (4) Karki, S.; Friščić, T.; Jones, W. *CrystEngComm* 2009, 11, 470–481.

317 (5) Fish, J. E.; Kemp, J. P.; Lockey, R. F.; Glass, M.; Hanby, L. A.; Bonuccelli, C. M. *Clin. Ther.*  
318 1997, 19, 675–690.

319 (6) Holohan, J. J.; Edwards, I. J. U.S. Patent 5,319,097, 1994.

320 (7) Anumula, R. R.; Gilla, G.; Alla, S.; Kurella, S.; Kopparapu, J. S. R.; Mediseti, R. K. V.;  
321 Maddula. S. R. U. S. Patent 20090149662 A1, 2009.

322 (8) Goldring, D.; Botoshansky, M.; Khalfin, R. L.; Pertsikov, B.; Nisnevitch, G.; Ponomarev, V.;  
323 Zaltzman, I.; Gutman, A.; Kaftory, M. *Acta Crystallogr., Sect. C: Cryst. Struct. Commun.* 2004,  
324 60, o843–o846. (9) Pastrano, G. L.; Ghaly, E. S. *Int. J. Pharm. Pharm. Sci.* 2012, 4,  
325 563–570.

326 (10) Sheldrick, G. M. *SHELXS: A Program for Automatic Solution of Crystal Structure*; University  
327 of Göttingen: Göttingen, Germany, 1997.

328 (11) Sheldrick, G. M. *Acta Crystallogr., Sect. A: Found. Crystallogr.* 2008, 64, 112–122.

329 (12) Hübschle, C. B.; Sheldrick, G. M.; Dittrich, B. J. *Appl. Crystallogr.* 2011, 44, 1281–1284.

330 (13) Best H-bond donor and acceptor groups according to Hunter's approach. Musumeci, D.; Hunter,  
331 C. A.; Prohens, R.; Scuderi, S.; McCabe, J. F. *Chem. Sci.* 2011, 2, 883–890.

332 (14) Forbes, C. C.; Beatty, A. M.; Smith, B. D. *Org. Lett.* 2001, 3, 3595–3598.

333 (15) Jabs, A.; Weiss, J. A.; Hilgenfeld, R. J. *Mol. Biol.* 1999, 286, 291–304.

334 (16) Bourn, A. J. R.; Gillies, D. G.; Randall, E. W. *Tetrahedron* 1964, 20, 1811–1818.

335 (17) Letavic, M. A.; Barberia, J. T.; Carty, T. J.; Hardink, J. R.; Liras, J.; Lopresti-Morrow, L. L.;  
336 Mitchell, P. G.; Noe, M. C.; Reeves, L. M.; Snow, S. L.; Stam, E. J.; Sweeney, F. J.; Vaughn,  
337 M. L.; Yu, C. H. *Bioorg. Med. Chem. Lett.* 2003, 13, 3243–3246.

- 338 (18) Haramoto, Y.; Yamada, T.; Nanasawa, M.; Funahashi, M.; Hanna, J.; Ujiie, S. *Liq. Cryst.* 2002,  
339 29, 1109–1111.
- 340 (19) de Boer, D.; Bosman, I. J.; Hidvégi, E.; Manzoni, C.; Benkö, A. A.; dos Reys, L. J. A. L.; Maes,  
341 R. A. A. *Forensic Sci. Int.* 2001, 121, 47–56.
- 342 (20) CSD refcodes: AFIGED, AYISIK, DIVCUH, DIVDOC, DIVMEB, EWAQOJ, ITIZOA,  
343 JEJGIP, LICFAE, LOHNOM, PIPERH, XOKBOO.
- 344 (21) Desikan, S.; Parsons, R. L., Jr.; Davis, W. P.; Ward, J. E.; Marshall, W. J.; Toma, P. H. *Org.*  
345 *Process Res. Dev.* 2005, 9, 933–942.
- 346 (22) Dunitz, J. D.; Bernstein, J. *Acc. Chem. Res.* 1995, 28, 193–200.
- 347 (23) Le Bail, A.; Duroy, H.; Fourquet, J. L. *Mater. Res. Bull.* 1988, 23, 447–452.
- 348 (24) Rodríguez-Carvajal, J. *Phys. B* 1993, 192, 55–69.
- 349 (25) Burger, A.; Ramberger, R. *Microchim. Acta* 1979, 72, 259–271.
- 350 (26) McCrone, W. C. In *Physics and Chemistry of the Organic Solid State*; Interscience Publishers:  
351 London, 1965; Vol. II.
- 352 (27) Chadwick, K.; Davey, R. J.; Dent, G.; Pritchard, R. G. *Cryst. Growth Des.* 2009, 9, 1990–1999.
- 353 (28) Shan, N.; Perry, M. L.; Weyna, D. R.; Zaworotko, M. J. *Expert Opin. Drug Metab. Toxicol.*  
354 2014, 10, 1255–1271.
- 355 (29) Lemmerer, A.; Adsmund, D. A.; Esterhuysen, C.; Bernstein, J. *Cryst. Growth Des.* 2013, 13,  
356 3935–3952.
- 357 .

358 **Legends to figures**

359

360 **Figure 1** Zafirlukast (ZF).

361

362 **Figure 2.** PXRD of the new solvates and anhydrous form of ZF.

363

364 **Figure 3** DSC and TGA of the ZF ACN solvate. DSC curve of the anhydrous form is shown for  
365 comparison.

366

367 **Fig. 4** DSC and TGA of the ZF BuOH solvate. DSC curve of the anhydrous form is shown for  
368 comparison.

369

370 **Figure 5.** Ribbons of self-assembled molecules of ZF in Form X.

371

372 **Figure 6.** (a) Cmethoxy–H $\cdots\pi$  interaction and (b) Carene–H $\cdots\pi$  interaction in Form X of ZF.

373

374 **Figure 7.** Self-assembled dimers of ZF stabilized by peripheral acetonitrile–amide interactions in ZF  
375 acetonitrile solvate (some hydrogens have been omitted for clarity).

376

377 **Figure 8.** Hydrogen bond interactions established between butanol and ZF molecules in the butanol  
378 solvate.

379

380 **Figure 9.** Chains of hydrogen-bonded molecules of ZF in the butanol solvate.

381

382 **Figure 10.** CH $\cdots\pi$  interactions observed in the butanol solvate.

383

384 **Figure 11.** Chains of ZF molecules in the piperazine cocrystal.

385

386 **Figure 12.** Cavity occupied by the piperazine molecule in the cocrystal (hydrogens and fragments of the  
387 ZF molecules have been omitted for clarity).

388

389 **Figure 13.** PXRD patterns of the five ZF/piperazine cocrystals.

390

391 **Figure 14.** PXRD patterns of the two 2:1 ZF/piperazine cocrystals.

392

393 **Figure 15.** Le Bail fit of 2:1 ZF/piperazine cocrystal Form B.

394 **Figure 16.** DSC and TGA traces of the 1:1 cocrystal Form C.

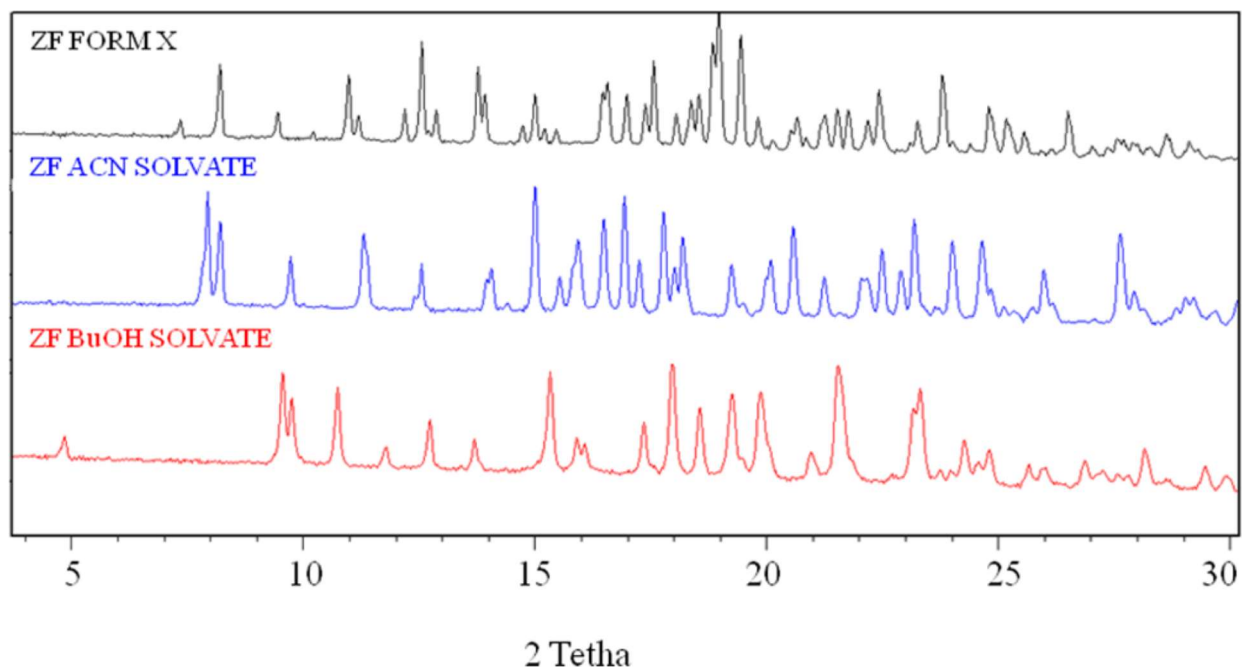
395

396



403  
404  
405

FIGURE 2

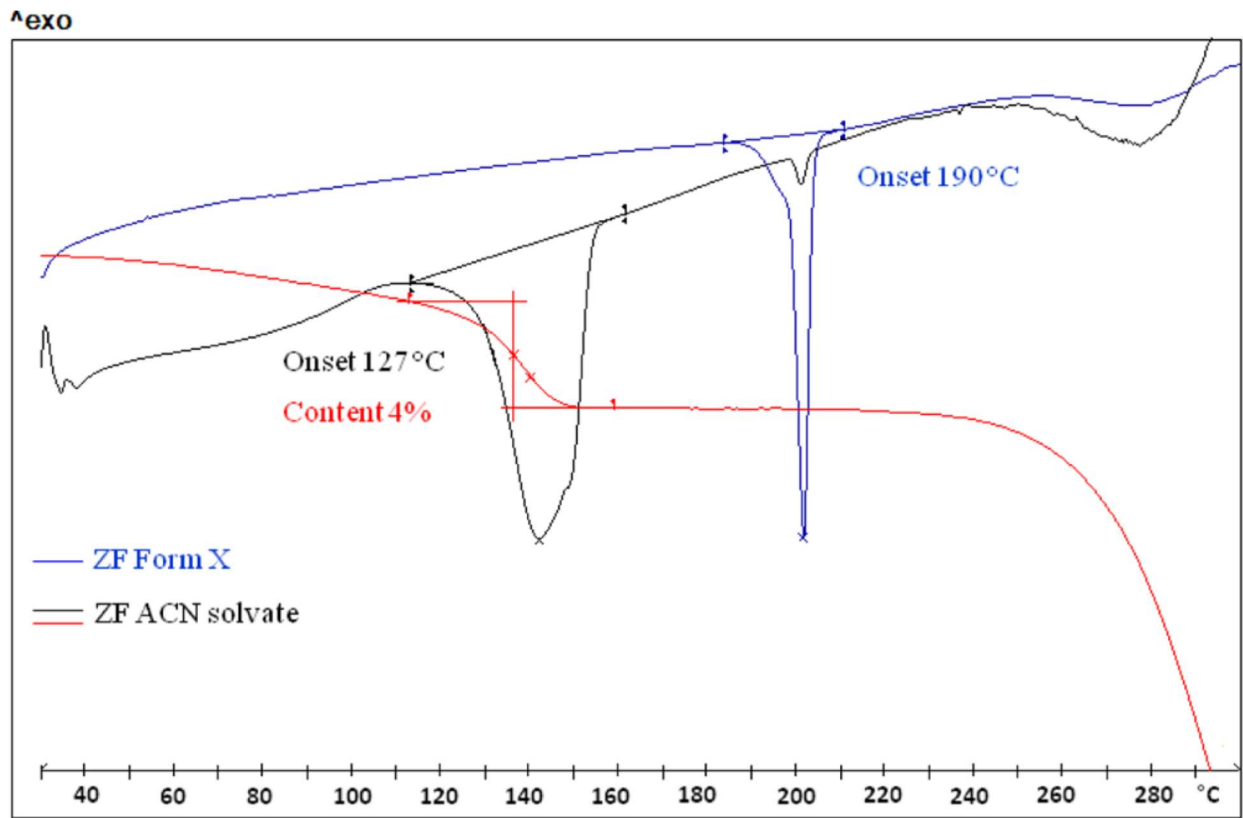


406  
407  
408  
409  
410  
411  
412  
413  
414



415  
416  
417

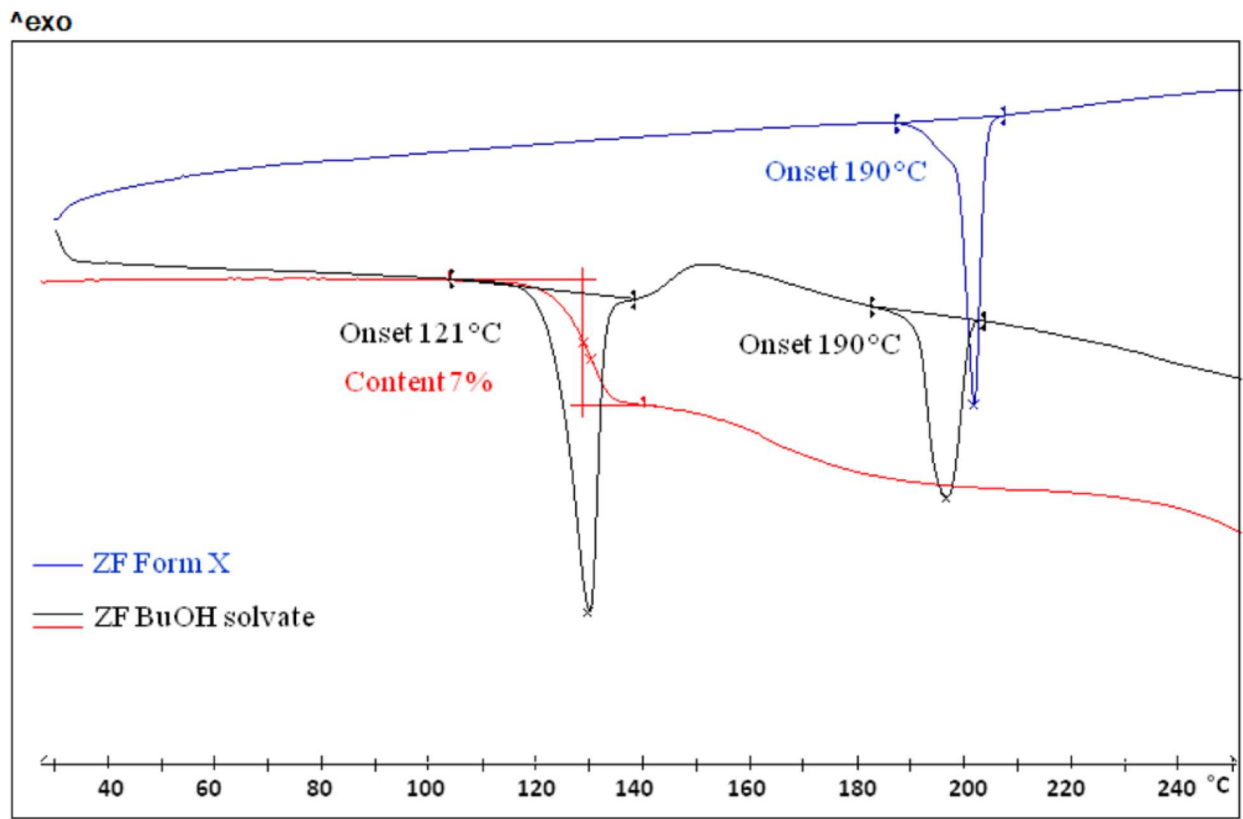
FIGURE 3



418  
419  
420  
421

422  
423  
424

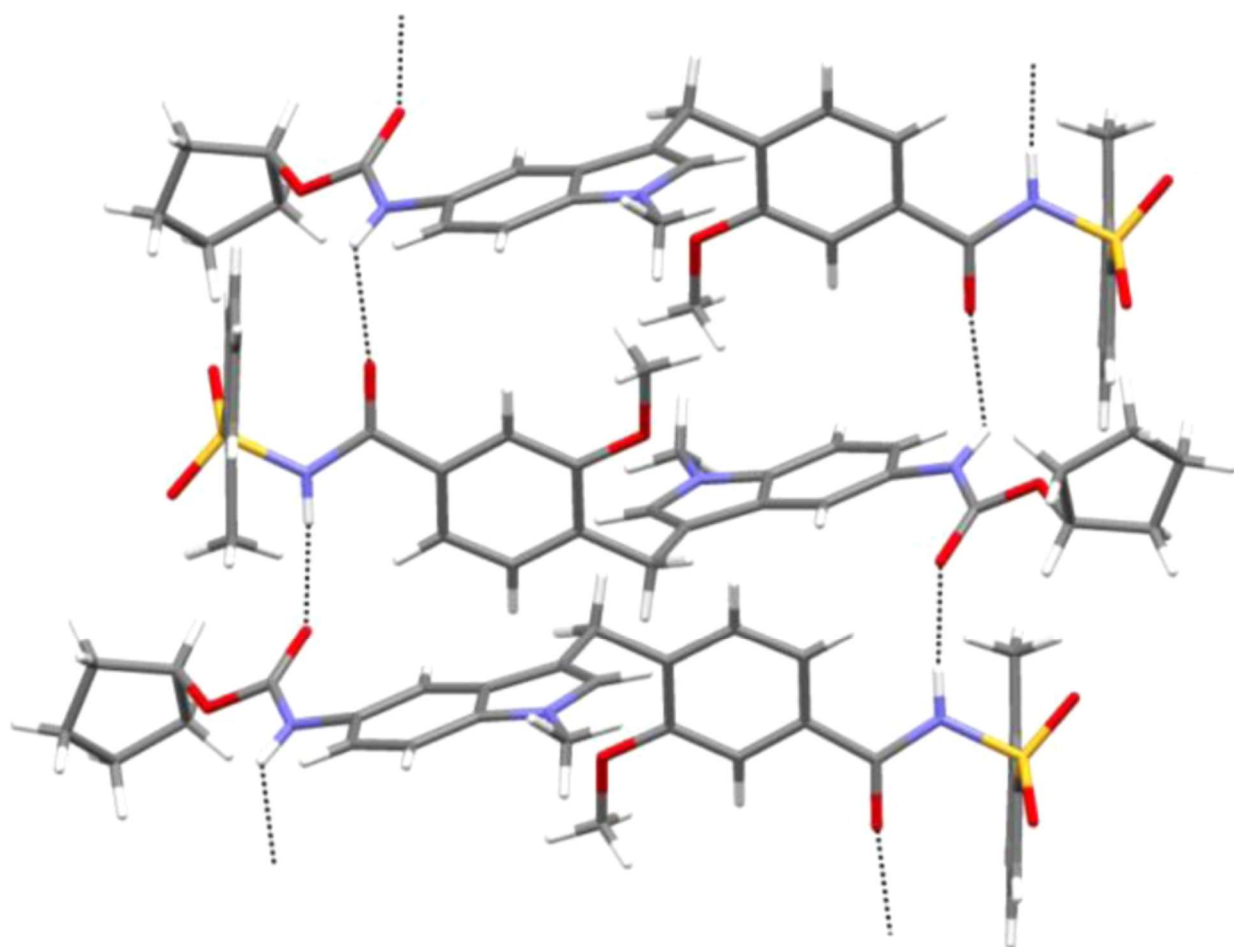
FIGURE 4



425  
426  
427  
428

429  
430  
431

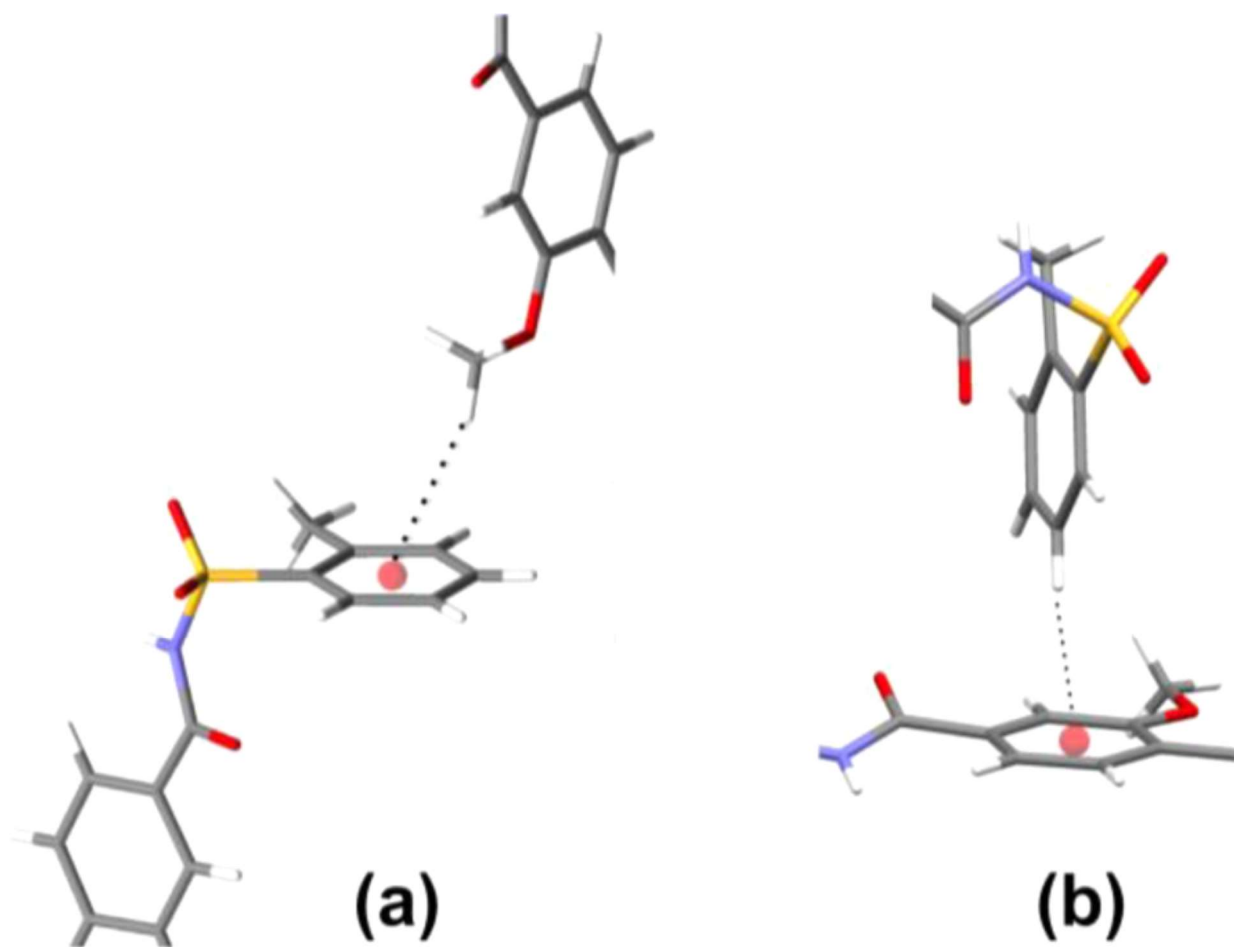
FIGURE 5



432  
433

434  
435  
436

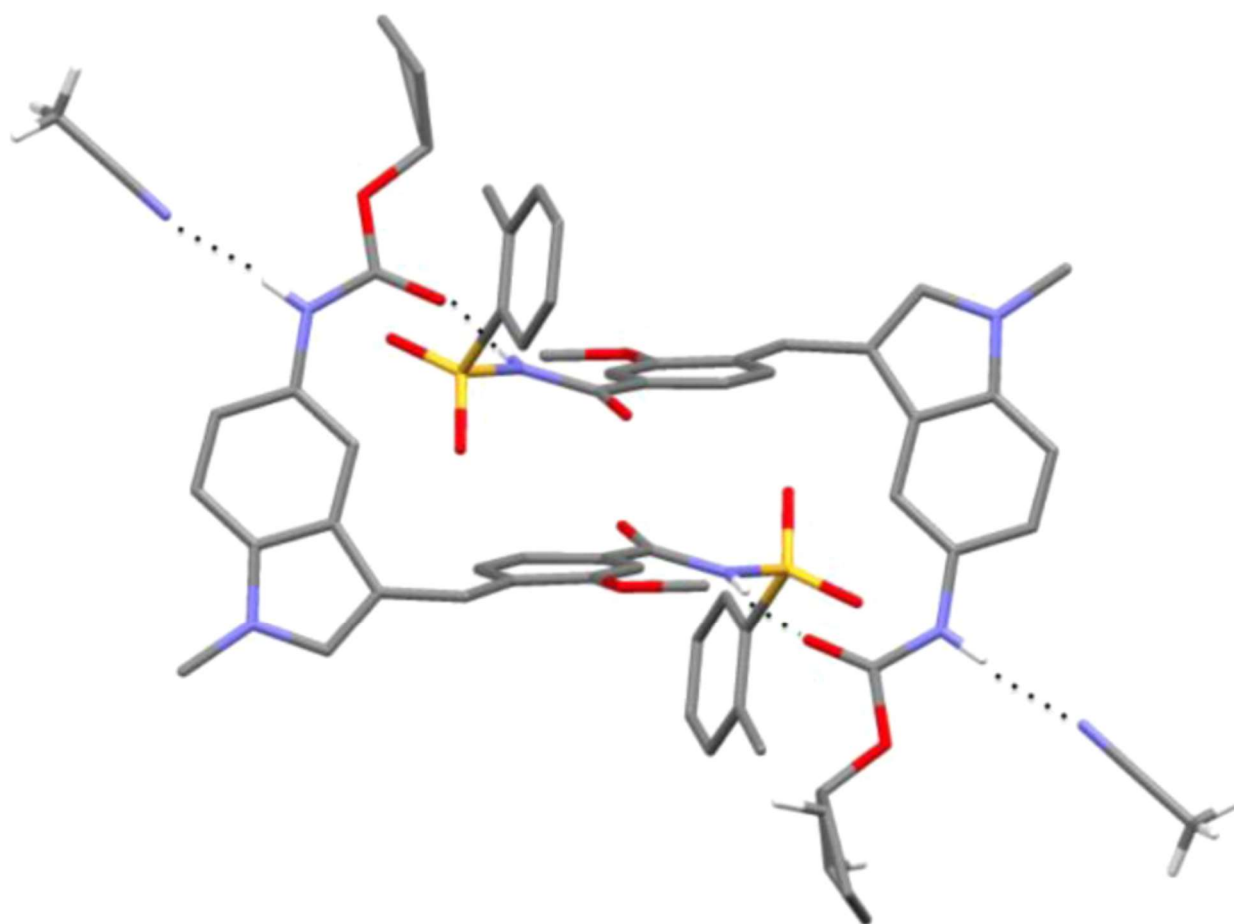
FIGURE 6



437  
438

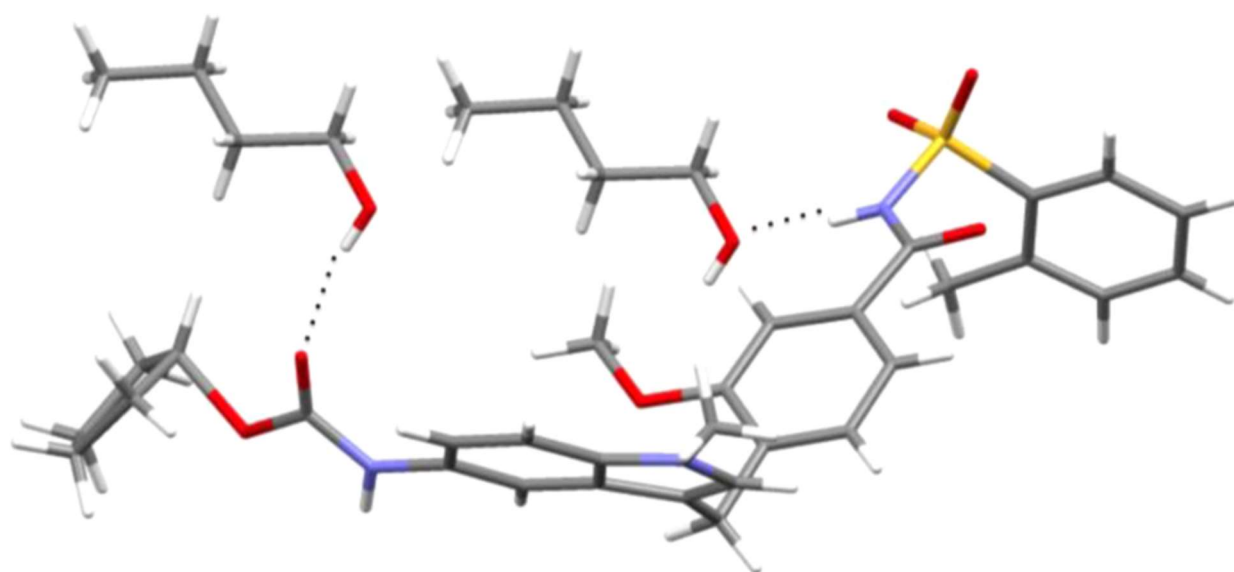
439  
440  
441

FIGURE 7



442  
443

FIGURE 8

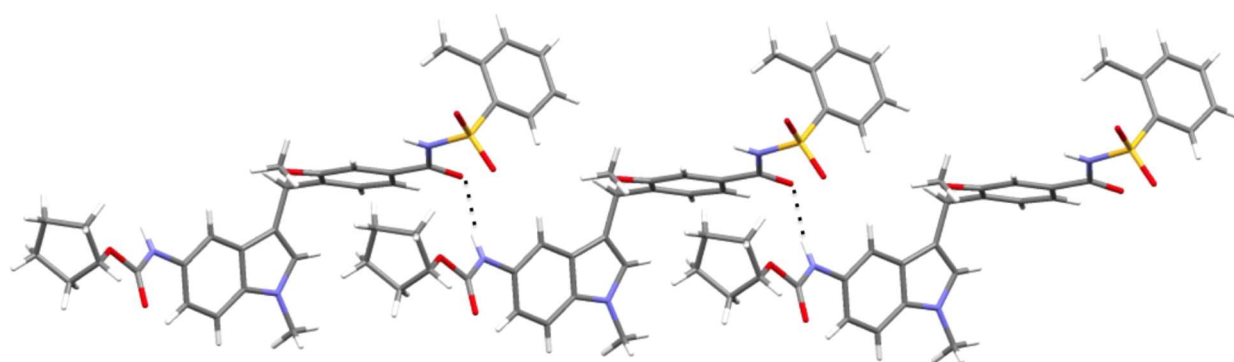


444  
445  
446

447  
448

449  
450  
451

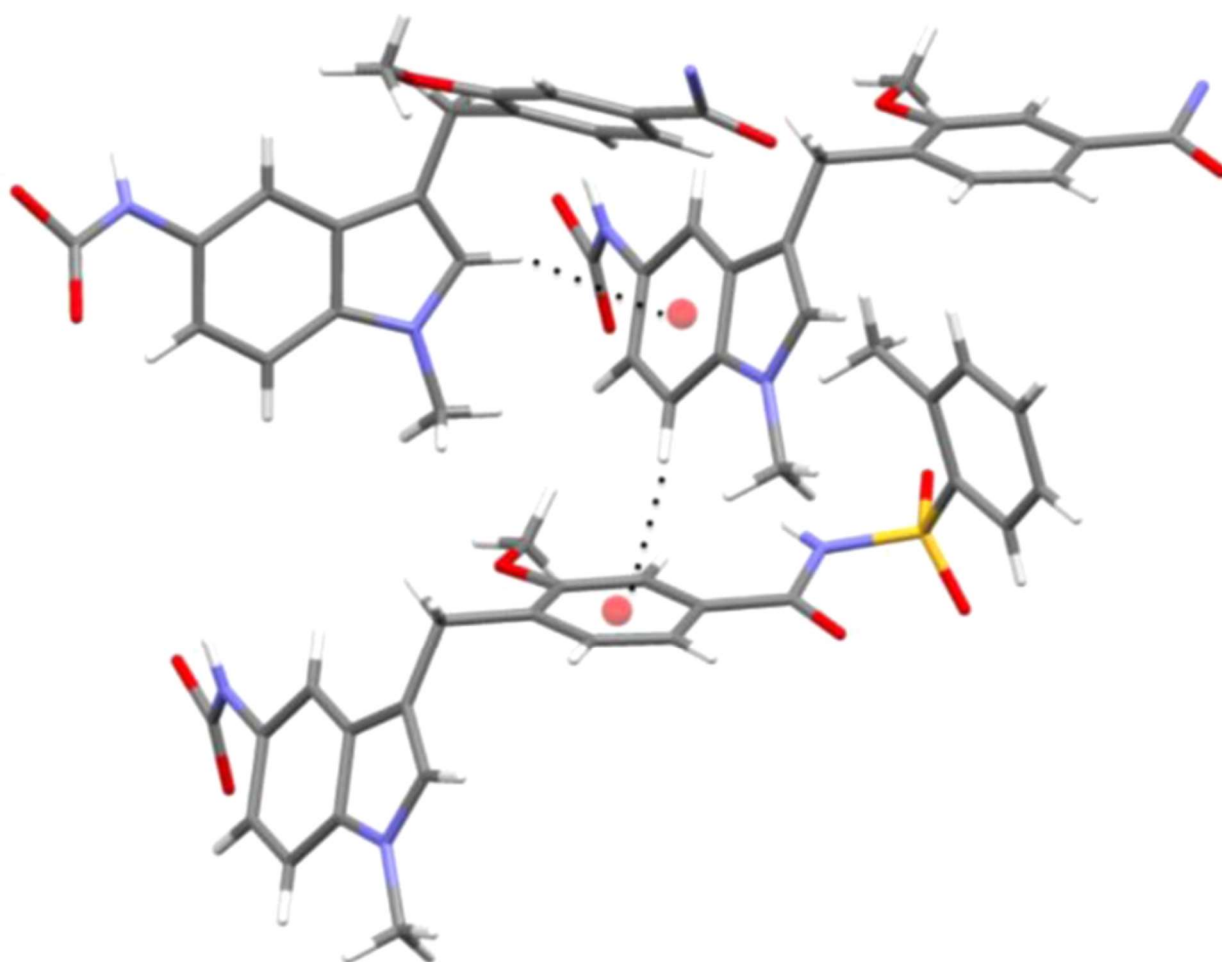
FIGURE 9



452  
453

454  
455  
456

FIGURE 10

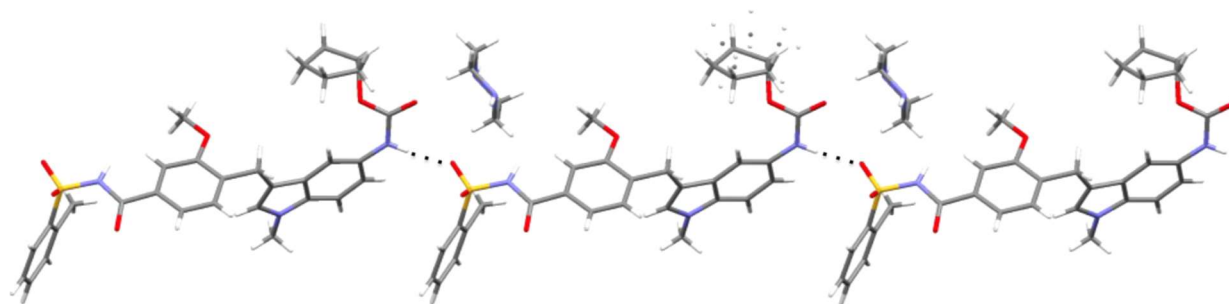


457  
458



459  
460  
461

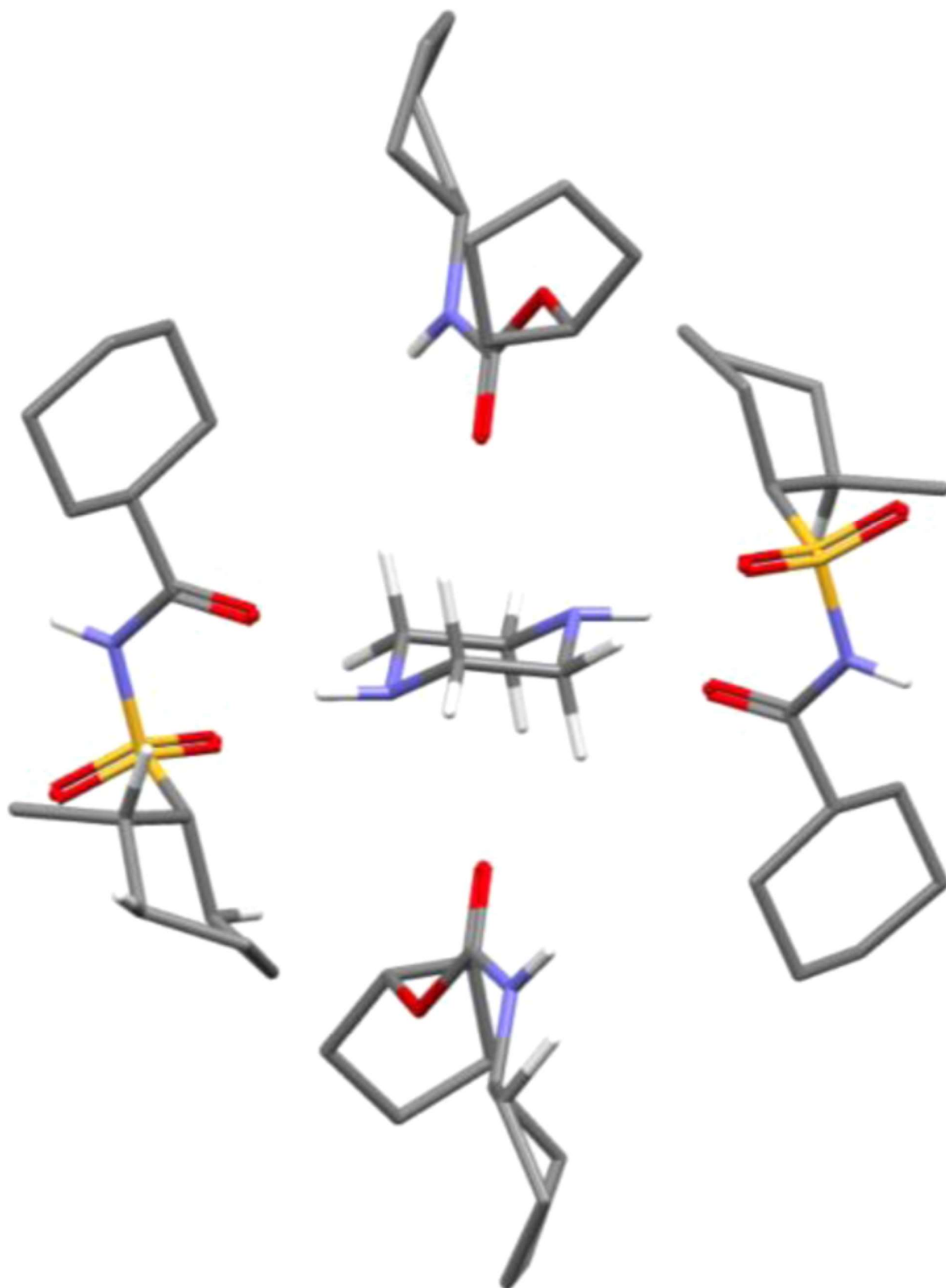
FIGURE 11



462  
463

464  
465  
466

FIGURE 12

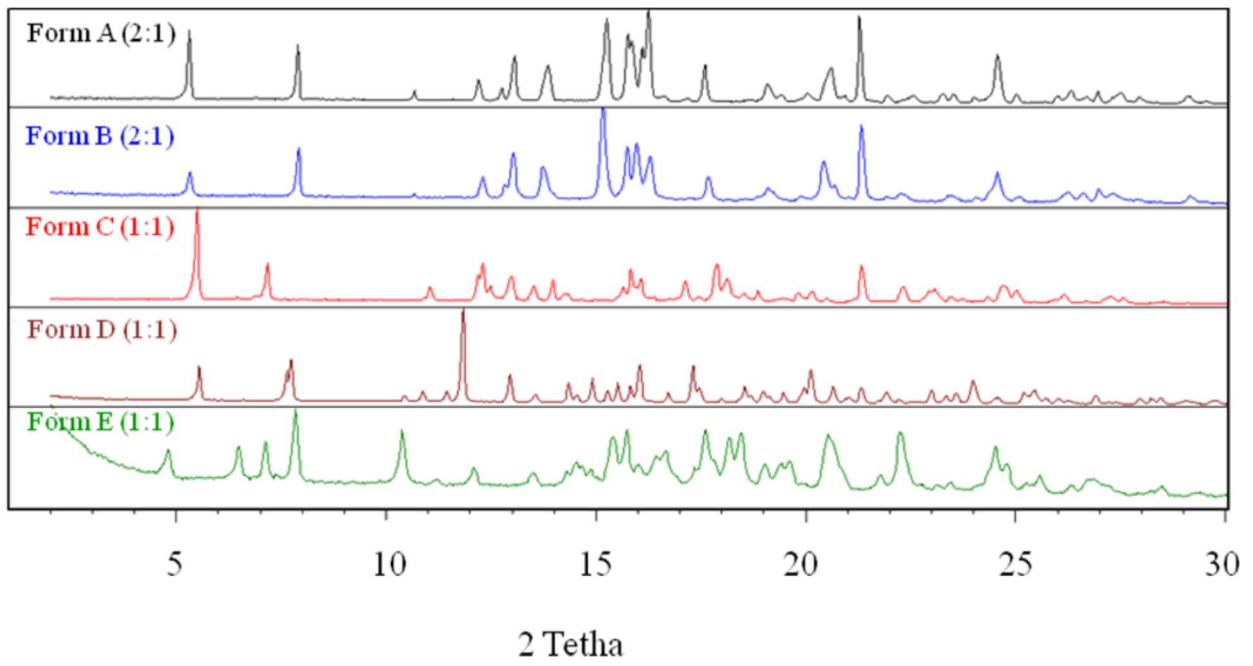


467



469  
470  
471

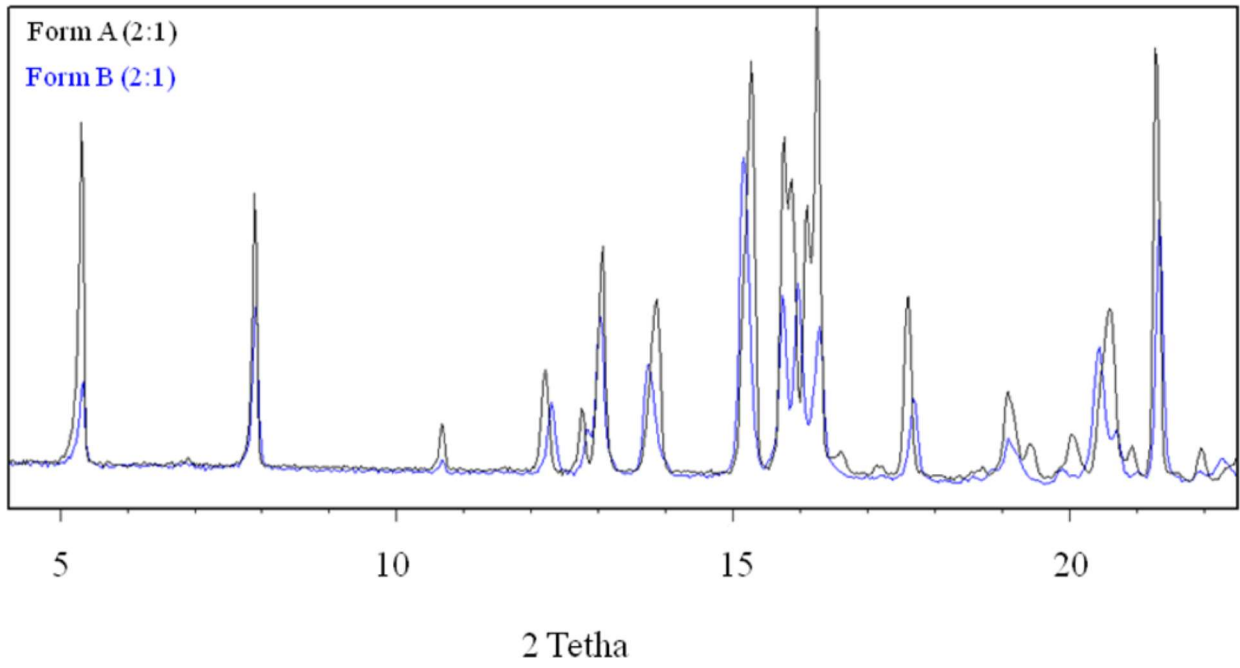
FIGURE 13



472  
473

474  
475  
476

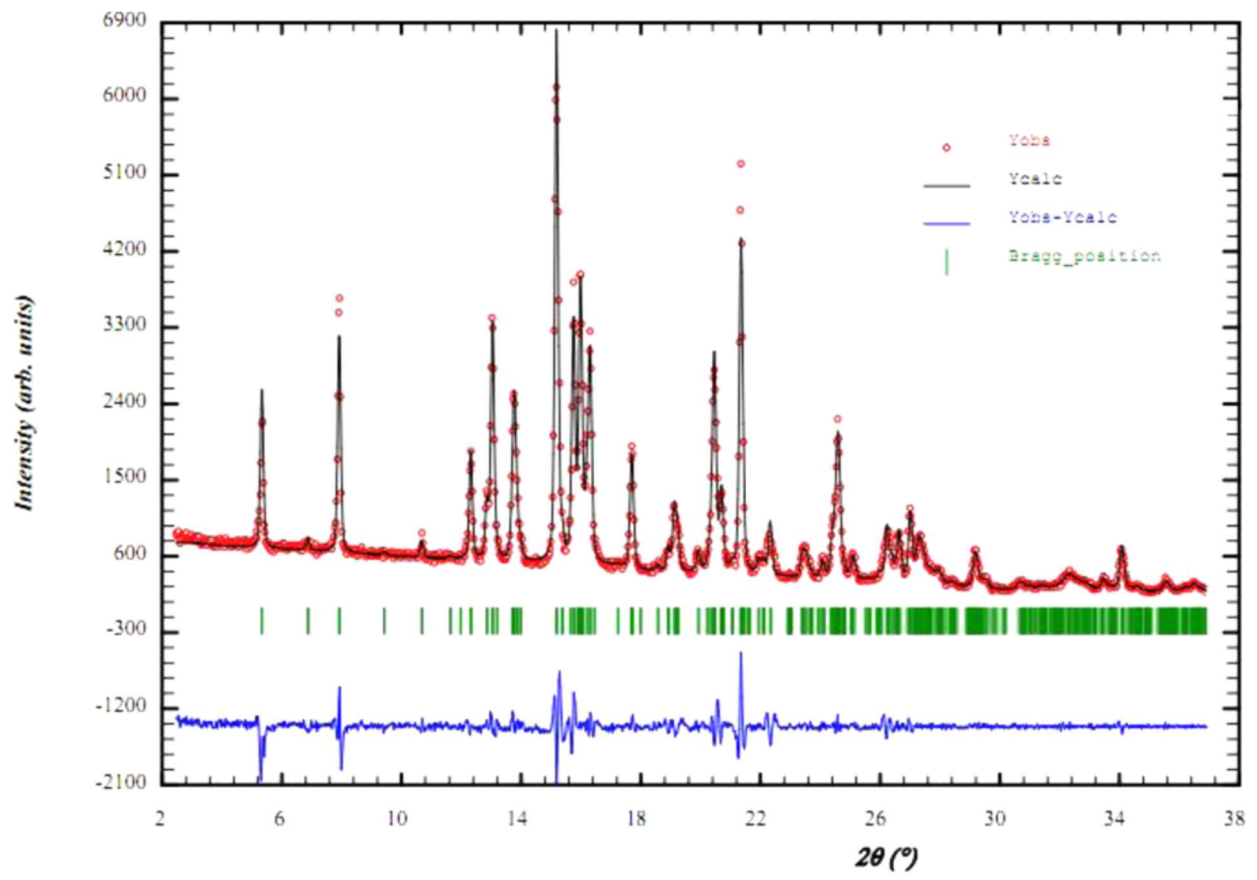
FIGURE 14



477  
478  
479

480  
481  
482

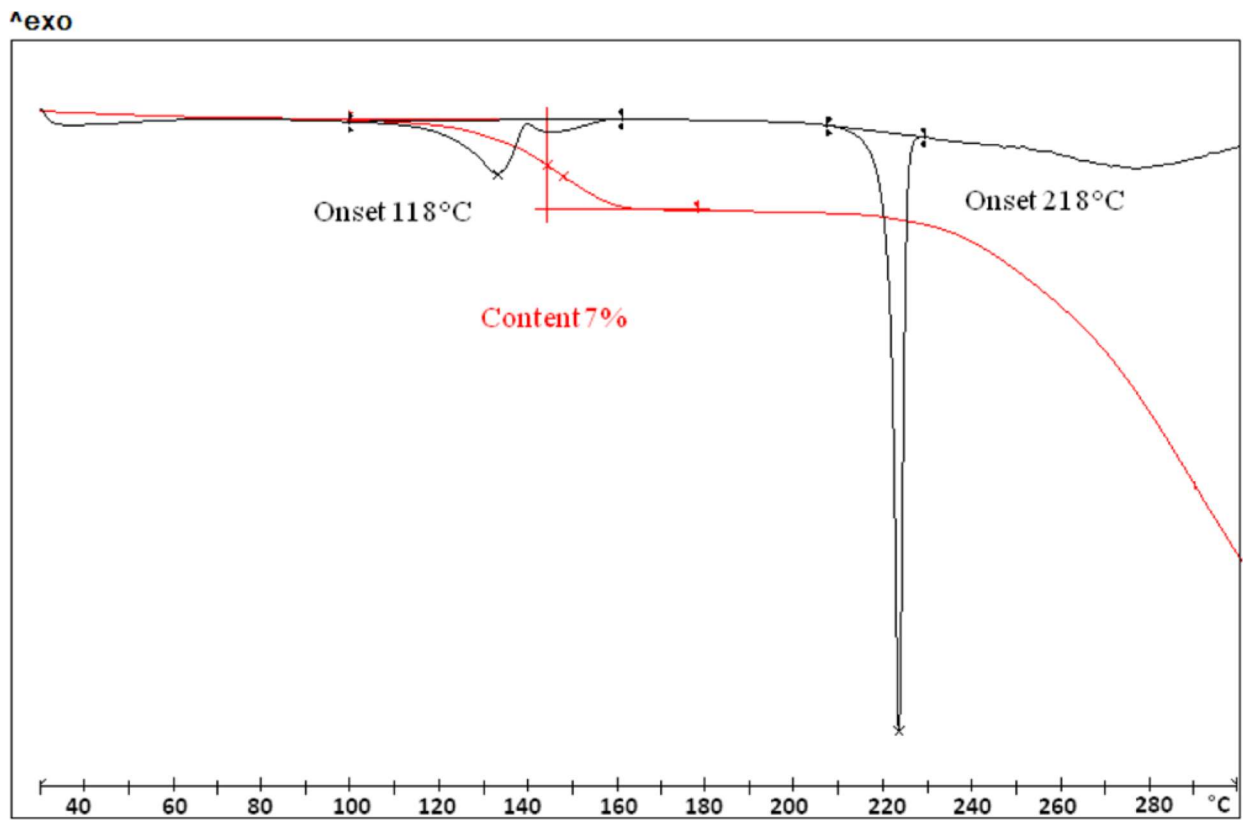
FIGURE 15



483  
484

485  
486  
487

FIGURE 16



488  
489

490 **Table 1.** Cell Parameters of the Two 2:1 ZF/Piperazine Cocrystals.

491

cell parameters <sup>a</sup>	Form A	Form B
a (Å)	7.65	16.86
b (Å)	13.40	13.47
c (Å)	16.80	7.62
$\alpha$ (deg)	78.77	75.84
$\beta$ (deg)	86.52	93.47
$\gamma$ (deg)	75.10	100.71
volume (Å <sup>3</sup> )	1631	1649
Z	2	2

<sup>a</sup>Both cells are triclinic (PT).

492

493

494

495

496



497 **Table 2** DSC Melting Data of the Two 2:1 ZF/Piperazine Cocrystal Polymorphsa

498

form	melting point (°C)	enthalpy of fusion (J/g)
A	218.12 ± 0.80	101.88 ± 5.52
B	212.23 ± 0.50	83.75 ± 5.65

<sup>a</sup>Values are the average ± standard deviation of three measurements at 10 °C/min under N<sub>2</sub>.

499

500

501

**Table 3.** Crystal Data and Structure Refinement Parameters for the Different Forms of ZF.

structure	form X	acetone:itile solvate	butanol solvate	piperezine cocrystal
empirical formula	$C_{10}H_{13}N_4O_5S$	$C_{10}H_{13}N_4O_5S$	$C_{10}H_{13}N_4O_5S$	$C_{10}H_{13}N_4O_5S$
formula weight	575.66	616.72	649.78	618.73
temperature (K)	293(2)	303(2)	302(2)	304(2)
wavelength ( $\text{\AA}$ )	0.71073	0.71073	0.71073	0.71073
crystal system	monoclinic	triclinic	monoclinic	triclinic
space group	$P2_1/c$	$P\bar{1}$	$C2$	$P\bar{1}$
$a, b, c$ ( $\text{\AA}$ )	9.578(9) 14.436 (10) 22.027(15)	11.7009(6) 12.3800(5) 12.8510(6)	10.333(4) 36.097(13) 9.961(3)	7.6482(14) 13.398(3) 16.798(3)
$\alpha, \beta, \gamma$ (deg)	90 102.557(14) 90	117.078(2) 98.813(3) 97.312(3)	90 112.768(12) 90	78.765(8) 86.517(8) 75.060(9)
volume ( $\text{\AA}^3$ )	2973(4)	1596(14)	3426(0)	1631(5)
$Z$ , density (calc) ( $\text{Mg/m}^3$ )	4, 1.286	2, 1.283	4, 1.260	1, 1.260
absorption coefficient ( $\text{mm}^{-1}$ )	0.156	0.151	0.146	0.148
$F(000)$	1213	652	1384	656
crystal size ( $\text{mm}^3$ )	$0.2 \times 0.1 \times 0.1$	$0.567 \times 0.299 \times 0.270$	$0.522 \times 0.140 \times 0.086$	$0.600 \times 0.205 \times 0.142$
$\theta$ range for data collection (deg)	1.699–32.301	2.246–27.550	2.211–28.815	2.197–27.628
limiting indices	$-12 \leq h \leq 12$ $-17 \leq k \leq 19$ $-31 \leq l \leq 29$	$-15 \leq h \leq 5$ $-16 \leq k \leq 16$ $-16 \leq l \leq 16$	$-13 \leq h \leq 13$ $-48 \leq k \leq 48$ $-13 \leq l \leq 11$	$-9 \leq h \leq 9$ $-17 \leq k \leq 17$ $-21 \leq l \leq 21$
reflections collected/unique	16526/5663 [ $R(\text{int}) = 0.0331$ ]	62499/7347 [ $R(\text{int}) = 0.0376$ ]	23746/7343 [ $R(\text{int}) = 0.0796$ ]	38980/7512 [ $R(\text{int}) = 0.01291$ ]
completeness to $\theta$ (%)	92.5	99.9	97.8	99.9
absorption correction	empirical	semiempirical from equivalents	semiempirical from equivalents	semiempirical from equivalents
max and min transmission	0.98 and 0.97	0.7456 and 0.7000	0.7457 and 0.6309	0.756 and 0.6345
refinement method	full-matrix least-squares on $F^2$	full-matrix least-squares on $F^2$	full-matrix least-squares on $F^2$	full-matrix least-squares on $F^2$
data/parameters	5663/2/349	7347/0/401	7343/5/397	7512/24/397
goodness-of-fit on $F^2$	1.149	1.026	0.915	1.030
final $R$ indices [ $I > 2\sigma(I)$ ]	$R_1 = 0.0558$ , $wR_2 = 0.1672$	$R_1 = 0.0515$ , $wR_2 = 0.1375$	$R_1 = 0.0247$ , $wR_2 = 0.0831$	$R_1 = 0.0809$ , $wR_2 = 0.1909$
$R$ indices (all data)	$R_1 = 0.0681$ , $wR_2 = 0.1744$	$R_1 = 0.0673$ , $wR_2 = 0.1518$	$R_1 = 0.1223$ , $wR_2 = 0.1042$	$R_1 = 0.1905$ , $wR_2 = 0.2429$
largest diff peak and hole ( $e\text{\AA}^{-3}$ )	0.661 and $-0.362$	0.311 and $-0.335$	0.233 and $-0.278$	0.441 and $-0.486$
CCDC	1062631	1062632	1062633	1062634